Selective Alkane Oxidation by Manganese Oxide: Site Isolation of MnO_x Chains at the Surface of $MnWO_4$ Nanorods

Xuan Li[a,b], Thomas Lunkenbein[a], Verena Pfeifer[a], Mateusz Jastak[a], Pia Kjaer Nielsen[a], Frank Girgsdies[a], Axel Knop-Gericke[a], Frank Rosowski[b,c], Robert Schlögl[a], and Annette Trunschke[a]*

Dedication ((optional))

Abstract: Electronic and structural properties of V-containing phases determine the isolation of active sites at the surface of catalysts for selective oxidation of alkanes. We show that this concept is not restricted to vanadium oxide. Deliberate use of hydrothermal techniques can turn the typical combustion catalyst Mn oxide into a selective catalyst for oxidative dehydrogenation of propane. Nano-structured, crystalline $MnWO_4$ serves as support that stabilizes a defect-rich MnO_x surface phase. Oxygen defects can be reversibly replenished and depleted at reaction temperature. Terminating MnO_x zigzag chains on (010) crystal planes are suspected to bear structurally site-isolated oxygen defects that account for the unexpected good performance of the catalyst in propane activation.

Prospective changes in the raw material basis in chemical industry to alternative feedstock bear new scientific challenges. This tackles, in particular, the area of oxidation catalysis where small saturated hydrocarbon molecules are going to be used as building blocks for olefins and aromatics.[1] The activation of inert C-H bonds in alkanes requires highly active catalysts. Often, high activity entails low selectivity due to over-oxidation of more reactive intermediates and desired products to CO and CO_2.[2] Vanadium oxide is the most prominent material that has been widely studied in selective oxidation of hydrocarbons and oxygenates.[3] Surface-sensitive *in-situ* experiments indicate that some well-known selective catalysts, composed of crystalline V-containing phases, are terminated by two-dimensional vanadium oxide layers.[4] These layers deviate in terms of composition and oxidation state of V significantly from the bulk crystal structure. The layer accounts for dynamic charge transfer between bulk and surface. This is reflected in the gas-phase-dependent response of the work function, electron affinity, and surface potential barrier, which was not found for the less selective bulk V_2O_5.[4i]

Herein, we conceptually verified that the selectivity of other unselective oxides, like Mn oxide, is also tunable by applying this extended site-isolation approach. We present the first example of a vanadium-free analogue that accomplishes efficient activation of propane by establishing a two dimensional Mn oxide layer in form of MnO_x chains at the surface of phase-pure, rod-shaped, nanostructured $MnWO_4$ (Figure 1, Figure S1). The catalyst was prepared by hydrothermal synthesis. The synthesis procedure reported previously,[5] was modified in the current work (description provided in the Supporting Information).

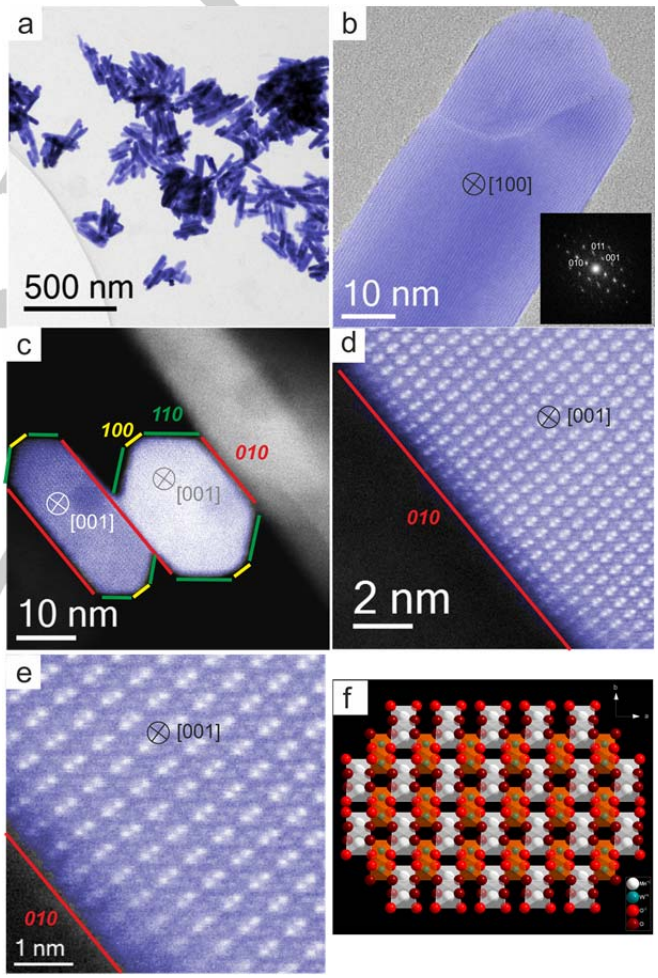

Figure 1. (S)TEM analysis of the $MnWO_4$ powder catalyst: a) Overview TEM micrograph of the $MnWO_4$ nanorods; b) HRTEM image of one nanorod particle viewed along [100]. The inset denotes the power spectra recorded on either side of the defect; c) HAADF-STEM image of condensed [001] oriented $MnWO_4$ nanorods. The surface termination was identified by phase analysis of corresponding atomic resolution HAADF-STEM images; d) and e) atomic resolution HAADF-STEM images of (c); f) Schematic representation of the crystal structure of $MnWO_4$ viewed along [001]. The Mn atoms are presented in white, W is coloured green and O atoms are displayed in red. The original images are given in the SI (Figure S1, 6c).

[a] X. Li, Dr. T. Lunkenbein, V. Pfeifer, M. Jastak, P.K. Nielsen, Dr. Axel Knop-Gericke, Dr. F.Girgsdies, Prof. Dr. Schlögl, Dr. A. Trunschke
Department of Inorganic Chemistry, Fritz-Haber-Institut der Max-Planck-Gesellschaft, Faradayweg 4-6, 14195 Berlin, Germany
E-mail: trunschke@fhi-berlin.mpg.de
[b] X. Li, Dr. F. Rosowski
BasCat – UniCat BASF Joint Lab, Technische Universität Berlin, Sekretariat EW K 01, Hardenbergstraße 36, 10623, Berlin, Germany
[c] Dr. F. Rosowski
BASF SE, Process Research and Chemical Engineering, Heterogeneous Catalysis, Carl-Bosch-Straße 38, 67056 Ludwigshafen, Germany

Supporting information for this article is given via a link at the end of the document.

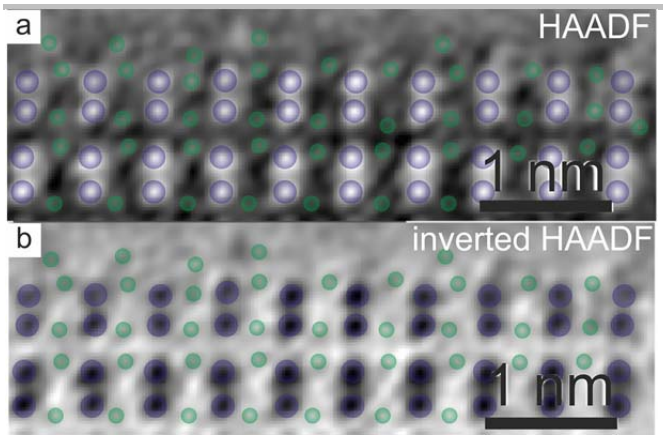

Figure 2. Surface termination of the *b* plane viewed along the growth direction [001] by FFT filtered atomic resolution STEM images a) HAADF, and b) inverted HAADF; The violet and green circles denote W and Mn atoms, respectively. The micrographs correspond to magnified images of Figure 1d. Original images are given in the SI (Figure S6).

Phase purity of the synthesis product was confirmed by Rietveld refinement of powder X-ray diffraction (Figure S2) applying anisotropic fitting. Transmission electron microscopy (TEM) imaging reveals typical rod-shaped nanoparticles with diameters varying from 13 to 51 nm (Figure 1 a-b, Figure S3) in agreement with XRD (Table S1). Fast Fourier transform (FFT) analysis of bright field TEM images of several particles (Figure S4) indicates in contrast to a former report[5] the preferential growth of the rods along the [001] direction. In addition, the power spectrum in Figure 1b reveals elongated spots, in particular for the (011) direction indicating a defective structure. Inverse Fast Fourier transformation (IFFT) of the 011 spots (Figure S5) indicates the occurrence of planar defects within the lattice. From the basal-area of two condensed nano-rods (Figure 1c) surface terminations can be distinguished that include (010), (110) and (100) planes. The atomic resolution high angle annular dark field- scanning transmission electron microscopy (HAADF-STEM) images (Figure 1d and e) viewed along [001] indicate the presence of two kinds of atomic dumbbells which can be distinguished by their different contrast. In HAADF-STEM the contrast is due to Rutherford scattering proportional to approximately Z^2. Thus, the dumbbells can be attributed to W_2O_8 (high contrast) and Mn_2O_y (less contrast) dimers. In the schematic representation of the $MnWO_4$ crystal structure (Figure 1f) the W_2O_8 and Mn_2O_y dimers are highlighted by orange and white colored edge-sharing octahedrons, respectively.

Atomic resolution HAADF-STEM images of the surface structure of the (010) plane viewed along [001] are shown in Figure 2 and illustrate a preferential surface exposure of Mn ions as unimers or dimers. The images indicate a slight out of center shift of some Mn ions compared to their bulk crystallographic position.

The Raman spectrum (Figure S7) of the nano-structured $MnWO_4$ agrees well with the spectrum of crystalline $MnWO_4$.[6] However, two additional, previously unreported bands appear at 615 and 665 cm^{-1}. Since phase purity and high crystallinity of the nano-structured material has been confirmed by TEM (Figure 1 and Figure S8) and XRD (Figure S2), these two bands are attributed to the MnO_x clusters at the surface of the nano-rods (Figure S9) that have been visualized by STEM (Figure 2).[7]

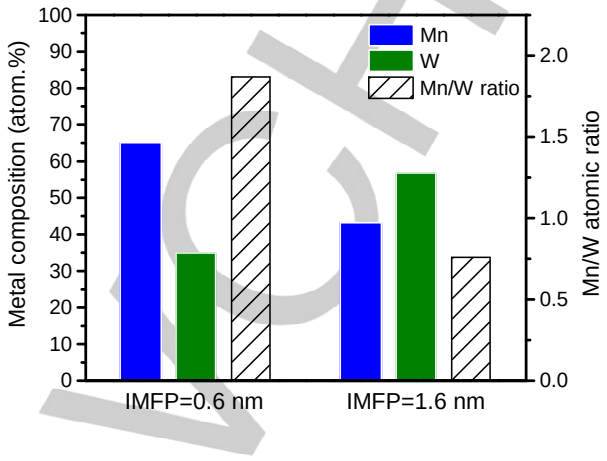

Figure 3. Depth profile of elemental composition of $MnWO_4$ nano-rods at two different depths represented by the inelastic mean free path (IMFP) of electrons measured by synchrotron-based NAP-XPS at T=300°C applying a total pressure of 0.25 mbar O_2 and He at flows of 2 and 2.2 sccm, respectively.

Synchrotron-based near ambient pressure X-ray photoelectron spectroscopy (NAP-XPS) reveals the enrichment of Mn on the outmost surface (Inelastic mean free path (IMFP) = 0.6 nm), within which the molar ratio of Mn to W is 1.9 (Figure 3). The Mn/W ratio decreases to 0.8 in the sub-surface region (IMFP = 1.6 nm) accordingly.

In summary, an enrichment of the surface of $MnWO_4$ nano-rods with manganese in the phase-pure, highly crystalline material was indicated by photoelectron spectroscopy. The specific surface termination is also reflected in the Raman spectrum. In line with these integral methods, the locally resolved atomic resolution HAADF-STEM images (Figure 2) present a partial Mn surface termination of the (010) planes. Thus, it is possible that the Mn enrichment observed by integral methods could be primarily attributed to an increased occurrence of the Mn terminated (010) planes (Figure 2) in the nano-structured material.

The specific surface / nano-structure of $MnWO_4$ is generated under hydrothermal conditions. *In-situ* Raman spectra taken during the synthesis (Figure 4) provide important information on the phase formation of $MnWO_4$. $MnWO_4$ nano-rods develop at around 125°C while the mixture of the aqueous solutions of Na_2WO_4 and $Mn(NO_3)_2$ is heated in the autoclave (Figure S10). An intermediate (910 cm^{-1}) is transformed to crystalline $MnWO_4$, indicated by the appearance of bands at 884, 325, 397, 510, 544, 672 and 698 cm^{-1}. The strongest band at 884 cm^{-1} has been assigned to the stretching mode of W=O in distorted WO_6 octahedrons.[6] Interestingly, two new bands at 615 and 665 cm^{-1} assigned to surface MnO_x clusters[7] grow in intensity with time when the synthesis temperature of 180°C has been reached. $MnWO_4$ crystallizes in a monoclinic structure (wolframite-type, ICSD-67906) in which WO_6 clusters form zigzag chains by

sharing edges along the [001] axis (Figure S9). In the basic medium under hydrothermal conditions (pH=9), WO_x clusters on the surface of the (010) planes could be dissolved due to the nucleophilic attack of OH^- ions at the bridging W-O-W bonds (Equation 1) leaving behind leached (010) surfaces composed of MnO_x zigzag chains. Subsequently, the bridging oxygen anions at the (001) surface may condense with the dissolved WO_4^{2-} monomers (shoulder at 926 cm^{-1} in Figure 4). Hence, the zigzag chains will propagate in one dimension by forming new O–W-O edge-sharing bridging bonds. Such a dissolution-recrystallization process may result in the observed anisotropic crystal growth along the [001] axis resulting in the rod-shaped morphology of the $MnWO_4$ particles enriched in MnO_x at the surface.

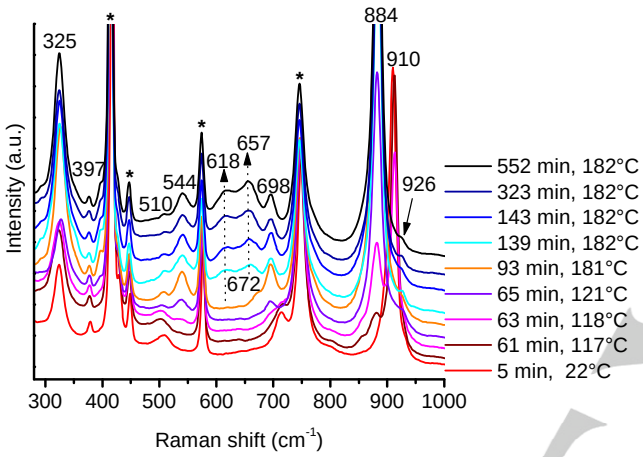

Figure 4. *In-situ* Raman spectra in the 280-1000 cm^{-1} range measured during hydrothermal synthesis of $MnWO_4$ nano-rods; Bands denoted with asterisks belong to the sapphire window of the Raman probe.

$$MnWO_4 + 2OH^- \leftrightharpoons Mn(OH)_2 + WO_4^{2-} \quad (1)$$

The nano-structured $MnWO_4$ material was studied as catalyst in oxidative dehydrogenation of propane. Conventional bulk crystalline $MnWO_4$ is rather inactive in the reaction, which is reflected in no measurable conversion at 450°C. Nano-structuring, however, as achieved by hydrothermal synthesis in the present work, can turn this material into an active catalyst exhibiting similar performance like silica-supported vanadium oxide (Figure 5). Moreover, the unique surface structure of the $MnWO_4$ nanorods exhibits superior selectivity to the desired product propylene than bulk manganese oxide. Manganese oxide is very active (Table 1), but not very selective and transforms propane almost completely into carbon oxides. Electronic modification and/or geometric separation of the MnO_x zigzag chains on the (010) planes by W_2O_8 units (Figure 2) apparently account for the improved performance. Propane conversion has been changed by varying the contact time at 400°C (Figue 5). The comparatively low temperature was chosen to avoid the influence of homogeneous gas phase reactions, which normally contribute to non-negligible conversion at elevated reaction temperatures above 450°C. The catalytic performance of $MnWO_4$ nano-rods reached steady state after 70 hours on stream and showed no sign of deactivation within 108 hours (Figure S11). Importantly, Mn terminating $MnWO_4$ nano-rods exhibit much higher apparent turnover frequency (TOF) than vanadium oxide species supported on silica (Table 1) when all Mn atoms at the (010) surfaces and all V atoms are taken into account as active sites. In reality, the number of active sites at the surface of the catalysts is, however, perhaps much lower.

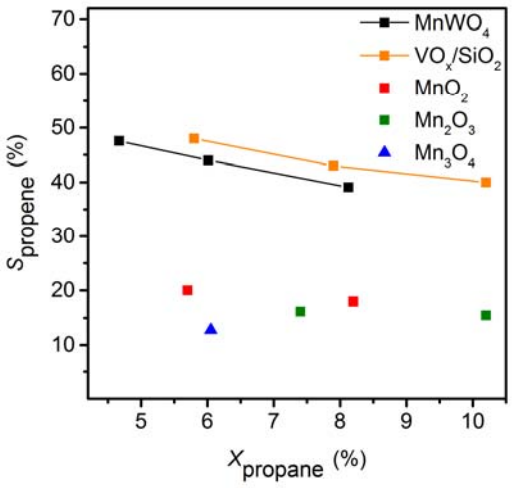

Figure 5. Catalytic performance of nano-structured $MnWO_4$ (T=400°C, W/F=1.8-0.9 g s/ml) in comparison to VO_x/SiO_2 (T=400-420°C, W/F=1.8 g s/ml) and various manganese oxides (T=330-395°C, W/F=1.8 g s/ml) in the oxidative dehydrogenation of propane in a feed composed of C_3H_8:O_2:N_2 in a ratio of 10:5:85. The selectivity to propene is shown as a function of propane conversion. Other C-containing products are mainly CO, and CO_2.

The Mn 2p XPS spectra (Figure S12) indicate the predominance of Mn in oxidation state two at the surface and within the subsurface. Tiny differences have been observed in the spectra under different reaction atmospheres (Figure S13), however, the interpretation of the Mn 2p spectra is not straightforward due to less distinct variations in the binding energies of compounds containing Mn in different oxidation states, an elaborate multiplet splitting, and the appearance of satellites.[8] In contrast, near edge X-ray absorption fine structure (NEXAFS) is sensitive to detect the surface oxidation of manganese oxides,[9] and changes in the coordination environment of the Mn ions.[10] The measured line shape of the Mn $L_{2,3}$-edge (Figure S14) agrees well with those from large single crystals of $MnWO_4$.[11] A predominance of Mn in oxidation state two is confirmed by the spectra both in oxygen and reaction atmosphere. Nevertheless, a small increase in the intensity ratio of the peaks at 640.0 and 641.4 eV has been observed during reaction (Table S2). With increasing oxidation state or, in other words, with increasing coordination of the Mn ions by oxygen atoms, intensity in the Mn $L_{2,3}$-edge spectrum occurs at higher energy.[9] Hence, the changes in the intensity ratio of the peaks at 640.0 and 641.4 eV indicate that in reaction

feed the concentration of oxygen defects is higher compared to oxygen atmosphere suggesting a substantial impact of oxygen defects on catalyst performance. Oxygen defects have been quantified by two temperature-programmed oxidation (TPO) and reduction (TPR) cycles (Figure S15). Before first TPO run, the catalyst was heated in Argon at 400°C for 2 hours. Approximately 3 oxygen atoms per nm^2 could be replenished after this treatment (Table S3). This underlines the notion[12] that only a fraction of surface atoms is catalytically active, which, however, holds great challenges in terms of the identification of active sites. The very similar hydrogen consumption profiles of the two TPR runs indicate that approximately 5% of the surface oxygen atoms were reversibly removed by reaction with H_2 (Table S3).

After washing with nitric acid solution and re-calcination under the same condition as that of the pristine $MnWO_4$ nano-rods, the catalytic activity decreased dramatically (Table 1). Only Mn was detected in the washing solution (Table S4). This further corroborates our argument that surface MnO_x chains are the active sites of the nano-structured $MnWO_4$ catalyst in oxidative dehydrogenation of propane.

In summary, we demonstrated that a catalytically inactive solid, like $MnWO_4$, was converted into a highly active and selective catalyst by knowledge-based synthesis. Hydrothermal techniques guided by *in-situ* spectroscopy[13] have been applied to control the surface termination. *In-situ* Raman spectroscopy provided insight into molecular processes of crystallization, surface dissolution and recrystallization under hydrothermal conditions. The unique self-supported structure of one-dimensional MnO_x clusters at the surface of nano-structured $MnWO_4$ demonstrates the importance of understanding the synthetic inorganic chemistry from a molecular point of view[14] and the significance of studying the surface termination[4d, 4e, 15] of well-defined nano-structured metal oxides[16]. By identification of the highly active surface MnO_x on the $MnWO_4$ nano-rods, the promotional effect of Mn in many catalytic systems could be better understood. The design of selective oxidation catalysts will benfit from this knowledge and it will lead to an improvement of current Mn doped catalytic systems.

Table 1. Active site density and reactivity of the catalysts in the oxidative dehydrogenation of propane at T=400°C, W/F=1.8 g s/ml in a feed composed of C_3H_8:O_2:N_2 in a ratio of 10:5:85.

Catalyst	$MnWO_4$ nano-rods	Acid washed-$MnWO_4$[a]	VO_x/SiO_2[b]	Mn_2O_3
rC_3H_8 /10^{-9}mol $m^{-2}s^{-1}$	8.69	2.46	0.27	550
Active site density /nm^{-2}	8.3[c]/3[d]	-	1.0	10.2[e]
TOF / $10^{-3}s^{-1}$	0.63/1.7	-	0.16	33

[a] treatment described in the Supporting Information; [b] VO_x supported on modified SBA-15 with a surface vanadium density of 1 V atom/nm^2; [c] Assuming that only MnO_x at (010) surface planes are active [d] Assuming that only oxygen defect sites at the surface are active sites [e] Mn density on the (100) plane.

Experimental Section

Hydrothermal synthesis and thermal activation procedures of $MnWO_4$ are described in detail in the Supporting Information. *In-situ* Raman measurements were performed applying a Kaiser Optics Raman Spectrometer RXN1 equipped with a fiber-optic probe head, using a laser wavelength of 785 nm. Additional experimental details of characterization techniques and catalytic tests are summarized in the Supporting Information.

Acknowledgements

This work was conducted in the framework of the BasCat collaboration between BASF SE, TU Berlin, FHI, and the cluster of excellence "Unified Concepts in Catalysis" (UniCat www.unicat.tu-berlin.de). X.L. acknowledges the Berlin International Graduate School of Natural Sciences and Engineering (BIG NSE) as part of UniCat for financial support. The authors thank Maike Hashagen, Jasmin Allan, Achim Klein-Hoffmann, Dr. Olaf Timpe, and Caroline Dessal for technical assistance. We thank the HZB staff for their continual support of the electron spectroscopy activities of the FHI at BESSY II.

Keywords: propane oxidative dehydrogenation •hydrothermal synthesis • in situ Raman • manganese tungstate • heterogeneous catalysis

[1] R. Schlögl, *Topics in Catalysis* **2011**, *54*, 627-638.
[2] F. Cavani, N. Ballarini, A. Cericola, *Catalysis Today* **2007**, *127*, 113-131.
[3] a) C. A. Carrero, R. Schloegl, I. E. Wachs, R. Schomaecker, *ACS Catalysis* **2014**, *4*, 3357-3380; b) K. Chen, A. Khodakov, J. Yang, A. T. Bell, E. Iglesia, *J. Catal.* **1999**, *186*, 325-333; c) K. Chen, E. Iglesia, A. T. Bell, *J. Catal.* **2000**, *192*, 197-203; d) T. Blasco, J. M. L. Nieto, *Applied Catalysis A: General* **1997**, *157*, 117-142; e) C. Hess, *ChemPhysChem* **2009**, *10*, 319-326; f) I. E. Wachs, *Dalton Transactions* **2013**, *42*, 11762-11769; g) B. M. Weckhuysen, D. E. Keller, *Catal. Today* **2003**, *78*, 25-46.
[4] a) M. Hävecker, R. W. Mayer, A. Knop-Gericke, H. Bluhm, E. Kleimenov, A. Liskowski, D. Su, R. Follath, F. G. Requejo, D. F. Ogletree, M. Salmeron, J. A. Lopez-Sanchez, J. K. Bartley, G. J. Hutchings, R. Schlögl, *J. Phys. Chem. A* **2003**, *107*, 4587-4596; b) M. Hävecker, A. Knop-Gericke, H. Bluhm, E. Kleimenov, R. W. Mayer, M. Fait, R. Schlögl, *Appl. Surf. Sci.* **2004**, *230*, 272-282; c) E. Kleimenov, H. Bluhm, M. Hävecker, A. Knop-Gericke, A. Pestryakov, D. Teschner, J. A. Lopez-Sanchez, J. K. Bartley, G. J. Hutchings, R. Schlögl, *Surf. Sci.* **2005**, *575*, 181-188; d) A. C. Sanfiz, T. W. Hansen, D. Teschner, P. Schno, F. Girgsdies, A. Trunschke, R. Schlo, M. H. Looi, S. Bee, A. Hamid, *J . Phys. Chem. C* **2010**, *114*, 1912-1921; e) M. Hävecker, S. Wrabetz, J. Kröhnert, L.-I. Csepei, R. Naumann d'Alnoncourt, Y. V. Kolen'ko, F. Girgsdies, R. Schlögl, A. Trunschke, *J. Catal.* **2012**, *285*, 48-60; f) M. Eichelbaum, R. Glaum, M. Hävecker, K. Wittich, C. Heine, H. Schwarz, C.-K. Dobner, C. Welker-Nieuwoudt, A. Trunschke, R. Schlögl, *ChemCatChem* **2013**, *5*, 2318-2329; g) C. Heine, M. Hävecker, M. Sanchez-Sanchez, A. Trunschke, R. Schlögl, M. Eichelbaum, *J. Phys. Chem. C* **2013**, *117*, 26988-26997; h) C. Heine, M. Hävecker, E.

Stotz, F. Rosowski, A. Knop-Gericke, A. Trunschke, M. Eichelbaum, R. Schlögl, *J. Phys. Chem. C* **2014**, *118*, 20405-20412; i) M. Eichelbaum, M. Hävecker, C. Heine, A. M. Wernbacher, F. Rosowski, A. Trunschke, R. Schlögl, *Angew. Chem. Int. Ed.* **2015**, *54*, 2922-2926; j) C. Heine, M. Havecker, A. Trunschke, R. Schlogl, M. Eichelbaum, *Phys. Chem. Chem. Phys.* **2015**, *17*, 8983-8993.

[5] S.-H. Yu, B. Liu, M.-S. Mo, J.-H. Huang, X.-M. Liu, Y.-T. Qian, *Adv. Funct. Mater.* **2003**, *13*, 639-647.

[6] a) L. H. Hoang, N. T. M. Hien, W. S. Choi, Y. S. Lee, K. Taniguchi, T. Arima, S. Yoon, X. B. Chen, I.-S. Yang, *J. Raman Spectrosc.* **2010**, *41*, 1005-1010; b) M. N. Iliev, M. M. Gospodinov, A. P. Litvinchuk, *Phys. Rev. B* **2009**, *80*, 212302.

[7] a) F. Kapteijn, A. D. Vanlangeveld, J. A. Moulijn, A. Andreini, M. A. Vuurman, A. M. Turek, J. M. Jehng, I. E. Wachs, *J. Catal.* **1994**, *150*, 94-104; b) F. Buciuman, F. Patcas, R. Craciun, D. R. T. Zahn, *Phys. Chem. Chem. Phys.* **1999**, *1*, 185-190.

[8] a) A. J. Nelson, J. G. Reynolds, J. W. Roos, *J. Vac. Sci. Technol., A* **2000**, *18*, 1072-1076; b) M. C. Biesinger, B. P. Payne, A. P. Grosvenor, L. W. M. Lau, A. R. Gerson, R. S. C. Smart, *Appl. Surf. Sci.* **2011**, *257*, 2717-2730.

[9] a) B. Gilbert, B. H. Frazer, A. Belz, P. G. Conrad, K. H. Nealson, D. Haskel, J. C. Lang, G. Srajer, G. De Stasio, *J. Phys. Chem. A* **2003**, *107*, 2839-2847; b) R. Qiao, T. Chin, S. J. Harris, S. Yan, W. Yang, *Curr. Appl. Phys.* **2013**, *13*, 544-548.

[10] S. P. Cramer, F. M. F. DeGroot, Y. Ma, C. T. Chen, F. Sette, C. A. Kipke, D. M. Eichhorn, M. K. Chan, W. H. Armstrong, *JACS* **1991**, *113*, 7937-7940.

[11] a) N. Hollmann, Z. Hu, T. Willers, L. Bohatý, P. Becker, A. Tanaka, H. H. Hsieh, H. J. Lin, C. T. Chen, L. H. Tjeng, *Phys. Rev. B* **2010**, *82*, 184429; b) K. V. Shanavas, D. Choudhury, I. Dasgupta, S. M. Sharma, D. D. Sarma, *Phys. Rev. B* **2010**, *81*, 212406.

[12] a) K. Amakawa, L. Sun, C. Guo, M. Hävecker, P. Kube, I. E. Wachs, S. Lwin, A. I. Frenkel, A. Patlolla, K. Hermann, R. Schlögl, A. Trunschke, *Angew. Chem. Int. Ed.* **2013**, *52*, 13553-13557; b) R. Schlögl, *Angew. Chem. Int. Ed.* **2015**, *54*, 3465-3520.

[13] M. Sanchez Sanchez, F. Girgsdies, M. Jastak, P. Kube, R. Schlögl, A. Trunschke, *Angew. Chem. Int. Ed.* **2012**, *51*, 7194-7197.

[14] R. Schlögl, S. B. Abd Hamid, *Angew. Chem. Int. Ed.* **2004**, *43*, 1628-1637.

[15] W. Zhang, A. Trunschke, R. Schlögl, D. Su, *Angew. Chem. Int. Ed.* **2010**, *49*, 6084-6089.

[16] A. Trunschke, in *Nanostructured Catalysts: Selective Oxidations*, The Royal Society of Chemistry, **2011**, pp. 56-95.

Entry for the Table of Contents (Please choose one layout)

Layout 1:

COMMUNICATION

Structural site isolation of surface manganese oxide species has been achieved by hydrothermal synthesis of nanostructured $MnWO_4$. In contrast to manganese oxide that is a combustion catalyst, MnO_x chains on the exposed (010) crystal planes of $MnWO_4$ selectively catalyse the oxidative dehydrogenation of propane to propene.

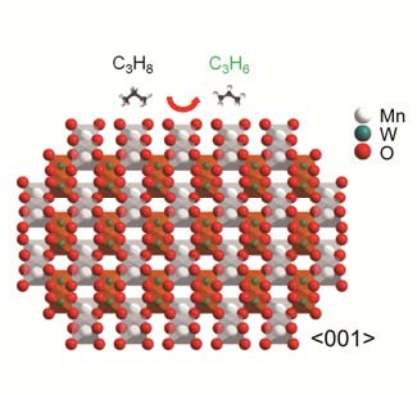

*Xuan Li, Dr. Thomas Lunkenbein, Verena Pfeifer, Mateusz Jastak, Pia Kjaer Nielsen, Dr. Frank Girgsdies, Dr. Axel Knop-Gericke,Dr. Frank Rosowski, Prof. Dr. Robert Schlögl, Dr. Annette Trunschke**

Page No. – Page No.

Selective Alkane Oxidation by Manganese Oxide: Site Isolation of MnO_x Chains at the Surface of $MnWO_4$ Nanorods